

Imaging a near-surface feature using cross-correlation analysis of multi-channel surface wave data

Kevin Samyn, Adnand Bitri, Gilles Grandjean

▶ **To cite this version:**

Kevin Samyn, Adnand Bitri, Gilles Grandjean. Imaging a near-surface feature using cross-correlation analysis of multi-channel surface wave data. Near Surface Geophysics, 2013, 11 (1), pp.1-10. 10.3997/1873-0604.2012007 . hal-00687133

HAL Id: hal-00687133
https://brgm.hal.science/hal-00687133

Submitted on 12 Apr 2012

HAL is a multi-disciplinary open access archive for the deposit and dissemination of scientific research documents, whether they are published or not. The documents may come from teaching and research institutions in France or abroad, or from public or private research centers.

L'archive ouverte pluridisciplinaire **HAL**, est destinée au dépôt et à la diffusion de documents scientifiques de niveau recherche, publiés ou non, émanant des établissements d'enseignement et de recherche français ou étrangers, des laboratoires publics ou privés.

Imaging a near-surface feature using cross-correlation analysis of multi-channel surface wave data

K. Samyn[1], A. Bitri[1], G. Grandjean[1]*

[1]BRGM, Bureau de recherches géologiques et minières, French Geological Survey, Risks Department, France

**Corresponding author:*

Kévin SAMYN

BRGM, Risks Department

3 Avenue Claude Guillemin BP36009 45060 Orléans Cedex 2, France.

Tel.: +33 (0)2 38 64 34 54.

Fax: +33 (0)2 38 64 36 89.

E-mail address: k.samyn@brgm.fr

Abstract

In this study, we demonstrate that cross-correlation gathers of multi-channel and multi-shot configurations provide accurate estimations of shear wave velocity (VS) perturbations from Rayleigh wave data for the reconstruction of two-dimensional (2D), high-resolution velocity distributions without requiring the systematic calculation of surface wave dispersions, as in the spectral analysis of surface waves (SASW). Data acquisition for cross-correlation analysis is similar to that for a 2D seismic common midpoint reflection survey. The data processing involved is similar to the coda wave interferometry used for seismological data but differs in the sense that the cross-correlation of the original waveform is calculated for active source seismic data. Data processing in cross-correlation analysis consists of the following three steps: First, cross-correlations are calculated for every trace in each shot gather with the same offset trace as a reference shot to flatten the linearly sloping events of surface waves. A common receiver location stack section can then be obtained, which allows for the assessment of lateral variations in the elastic properties of the medium. Second, the maxima of the time-shifted cross-correlation gathers and the maxima of the shot gathers' envelope traces are picked for different frequencies, and trace values having the same receiver location are averaged to calculate Vs perturbations, as described in the theory of coda wave interferometry. Finally, a 2D Vs profile is reconstructed by applying the lateral Vs perturbation to a homogeneous Vs velocity profile obtained by inversion of the surface wave dispersion of the reference shot gather. Analyses of waveform

data from numerical modelling and field observations indicate that this new method is valid and greatly improves the accuracy and resolution of near-surface imagery using surface waves and reconstructed subsurface velocity distributions compared with a conventional SASW or multi-channel application.

Keywords

surface wave, cross-correlation, shear-wave velocity (Vs)

Introduction

The delineation of shear wave velocity (Vs) structures down to a depth of approximately 30 m is of fundamental interest in engineering and environmental problems. P-wave and S-wave (PS) velocity logging has been adopted for this purpose for a number of years. The expense of drilling a borehole and operating a logging tool has led to a demand for more convenient methods for determining shallow surface wave structures. It is well known that the dispersion of the phase velocities of surface waves is mainly determined by the ground structure. The use of surface waves for near-surface delineation has been the subject of many studies in the past decade. For example, the spectral analysis of surface waves (SASW) has been used for the determination of 1D Vs structures down to a depth of 100 m (Nazarian *et al*. 1983; Stokoe *et al*. 1989; Grandjean and Bitri 2006). The majority of the surface wave methods described to date employ a shaker or a vibrator as a wave source and exploit calculated phase differences between two receivers using a simple cross-correlation technique. Park *et al.*, 1998a and Debeglia *et al*. (2006) also discuss the feasibility of detecting near-surface features using dynamic linear moveout (dlmo) for surface wave imagery. A multi-channel analysis of surface waves (MASW) has been proposed by several authors (Song *et al*. 1989; Park *et al*. 1999a; Xia *et al*. 1999). This method determines phase velocities directly from multi-channel surface wave data after applying an integral transformation to the frequency-domain waveform data. The integration directly converts time-domain waveform data (time-distance) into an image of phase velocity versus frequency

(*c*–*f*). Hayashi *et al*. (2004) show that the accuracy and resolution of (*c*-*f*) images can be improved using common mid-point (CMP) cross-correlation analysis of multi-channel surface wave data. The MASW method is more effective than the SASW method because MASW allows the fundamental mode of Rayleigh wave dispersion to be distinguished visually from body waves and from higher modes of the Rayleigh waves. Additionally, the MASW method avoids spatial aliasing, which is a problem in the SASW method (Foti *et al*. 2001; Neducza 2007). Xia *et al*. (2005) and Miller *et al*. (1999) applied the MASW method to continuous-profiling shot records and delineated 2D Vs structures and their resolution to determine phase velocities at low frequencies. Importantly, Park *et al*. (1999a) noted that it is essential for the MASW method to use a receiver array that is as long as is practical. However, a longer receiver array can decrease the lateral resolution of a survey because the conventional MASW method provides a velocity model averaged over the total length of the array. We developed a novel method to address this trade-off. Developing an alternative to conventional surface wave methods for the determination of lateral variations in Vs structure required a unique approach based on the multi-channel recording of surface waves and a cross-correlation analysis.

Surface wave response to a near-surface feature

A near-surface anomaly is defined here as a component of the near-surface materials that has elastic properties differing significantly from those of the

remaining components, which are termed normal zones. The transition from a normal to anomalous zone may be either abrupt or gradual. During a surface waves survey, a near-surface anomaly leaves a signature of its presence in several forms on a multi-channel recording, the most common form being different phase velocities for those frequencies propagating through or near the anomaly; another form consists of differing attenuation characteristics.

In addition to differing phase velocities and attenuation characteristics, an anomaly may reveal its presence in the form of the generation of higher modes (Bath 1973; Gucunski and Woods 1991), or reflected and diffracted (Yanovskaya 1989; Sheu *et al*. 1988) surface waves. The generation of these higher modes is closely related to the existence of a low-velocity zone underlain by and overlying high-velocity zones (a zone of velocity inversion) (Stokoe *et al*. 1994), and the energy of the higher modes typically becomes more significant at high frequencies (short wavelengths) (Tokimatsu *et al*. 1992). Reflected and diffracted surface waves are generated when the transition from normal to anomalous zones is abrupt. All of these anomaly signature types may appear on a multichannel record when either the source or the receivers are located at or near the surface location of an anomaly.

Theoretically, surface waves cannot penetrate through a void filled with air or fluid because of the lack of shear modulus inside the void. However, considering the retrograde elliptical motion of mass underneath a roll disturbance, the surface waves that penetrate above and below the void with dimensions of elliptical motion that significantly exceed the dimensions of the

void may still propagate horizontally but with altered propagation characteristics with respect to attenuation, variations in phase velocity, or both.

Methodology

Principles

To improve the lateral resolution of multichannel surface wave methods, we considered the Vs perturbation relative to a reference shot gather through the cross-correlation of Rayleigh wave shot gather data recorded at different positions along a line. Cross-correlation is a standard method of estimating the degree to which two series are correlated. The cross-correlation function, *R(Δt)*, represents the correlation coefficient between two seismic signals at time *t = 0, S(0)*, and a later time *t*, *S(t)*. The cross-correlation function can be expressed as follows:

$$R(\Delta t) = \frac{\sum_{i=0}^{M-m} S_1(i\tau) S_2(i\tau + m\tau)}{\langle S_1 \rangle \langle S_2 \rangle (M-m)} \qquad (1)$$

where m is an integer multiple of a time interval, τ, such that $\Delta t = m\tau$ (where $0<m<M$). $S_1(t)$ and $S_2(t)$ are the time-dependant surface wave signals from traces 1 and 2, respectively. Both traces comprise M+1 data points spanning the period from t=0 to $t=M\tau$. $\langle S_1 \rangle$ and $\langle S_2 \rangle$ are the mean intensities of the surface wave signal in traces 1 and 2, respectively.

Herein, we compare the surface wave signals. Our goal is to determine whether the two signals are correlated (i.e., fluctuating in concert) or uncorrelated (fluctuating independently). In modelling the autocorrelation in time, we assume that the correlation of a surface wave signal with itself decays from a perfect correlation at time zero to no correlation at infinite time. For the cross-correlation between two surface wave signals at different locations, assuming seismic source repeatability, near-surface features and near-surface Vs structures create perturbations, and the two signals then fluctuate independently; thus, the correlation between them decays at a certain propagation time.

Cross-correlation temporally correlates the intensity fluctuations of the seismic traces. In cross-correlation, only pairs of coherent samples from two distinct traces appear as a positive result at time t, whereas fluctuations in the surface wave signal created by a Vs perturbation generate a positive result at time $t+dt$, accounting for the travel-time perturbation dt.

On a simplistic level, cross-correlation analysis is coincidence analysis. The cross-correlation function between traces therefore enables a determination of the manner in which the Vs structure varies in the near surface.

Data processing procedure

A cross-correlation analysis of surface waves (CCASW) is applied to each shot gather in the dataset. Data acquisition for the CCASW method is similar to that

for a 2D seismic common midpoint reflection survey. The source-receiver geometry is based on the end-on spread, and both the source and the receivers move up along a survey line. The processing for the CCASW is summarised in the following:

First, cross-correlations are calculated for every trace in each shot gather along the entire seismic line using the same offset trace of a user-selected reference shot gather from the overall dataset, which is considered to be unperturbed. The reference location is a presumably normal zone within the survey line. The cross-correlation process allows us to correct for the offset effect and therefore, to flatten the linearly sloping events of surface waves in the same way as a dlmo (Park *et al*. 1998a, b). All of the common receiver location traces in cross-correlated shot gathers can then be stacked together. The above procedure achieves the following effects after stacking:

• Frequencies that have the same phase velocity as that at the reference location will have large stacked amplitudes due to constructive interference.

• For those shot gathers obtained at or near the surface location of an anomaly, cross-correlation will result in time-shifted stacked traces or weak amplitudes traces due to destructive interference.

• All of the higher modes will be attenuated through destructive interference due to their different phase velocities.

• All non-planar, body waves will be attenuated due to destructive interference because of their nonlinear occurrence on a multi-channel record or because of wrong velocities used for moveout correction.

185 • All reflected surface waves will appear as diffractions in the final stack section.

186 • Random noise will be attenuated.

187 When the stacked traces are displayed, all of the normal zones will show large
188 amplitudes, and the anomalous zones will be denoted by diffractions,
189 attenuated amplitudes or time-shifted events. Such a stack section is thus a
190 good method to obtain an initial view of the lateral variations in elastic properties
191 along the survey line.

192 To quantify the observations made on the stack section, we then applied coda
193 wave interferometry to our active source survey, stipulating that a
194 homogeneous relative change in seismic velocity, *dv/v,* results in a time-shift *dt*
195 (Snieder *et al*. 2002; Wegler and Sens-Schönfelder 2006) of:

196 $$dt = -t\frac{dv}{v} \qquad (2)$$

197 For this purpose, the maxima of the cross-correlated gather is then picked to
198 obtain the travel-time perturbation *dt*, and the maxima of the shot gather's
199 envelope traces are used to obtain the surface wave travel time, *t*. The trace
200 envelope is an attribute of seismic traces computed using the function
201 suattributes of the Seismic Unix (SU) package and corresponds to the envelope
202 amplitude of the trace.

203 These two variables are inserted into equation (2) to calculate the Vs
204 perturbations *dv/v*. The Vs perturbations with the same receiver location are
205 averaged. A Vs profile is reconstructed by applying the velocity perturbation

model at different frequencies to a homogeneous Vs profile obtained by inversion of the surface wave dispersion of the reference shot gather.

Numerical modelling

Two numerical tests were performed to evaluate the proposed method. Fig. 1 shows the source-receiver configuration used for data acquisition. Fig. 2 shows the velocity models used for numerical modelling. Both directions of the moving-source observations of surface waves on the survey line were tested. The two models are composed of a homogeneous half-space with Vp=1200 m/s and Vs=600 m/s and a low-velocity, vertical and buried defect with Vp=1000 m/s and Vs=500 m/s. The Seismic Unix (SU) suea2df function (Juhlin, 1995), which is based on a stress-velocity, staggered grid, 2D finite-difference method (Levander, 1988; Virieux, 1986), was used for the waveform calculation. Synthetic seismic gathers were generated using a zero-phase Ricker wavelet. The finite difference calculation was performed using 321 and 213 0.5 × 0.5 m cells, respectively, for the x and z axes and 12000 samples with a sample interval of 0.1 ms. The synthetic model size was chosen to be sufficiently large to get free from border effects. After the calculations, the data were resampled to 48 traces with 1 m spacing and 1000 samples with a 1 ms sample interval and processed using CCASW.

Fig. 3 presents a flow diagram illustrating the processing procedure for the synthetic shot gather data obtained through numerical modelling. Fig. 3a

illustrates the cross-correlation operation for selected synthetic examples. The variables *dt*, *t,* and *dv/v* are highlighted in Figure 3b.

Figs. 4a, 4b, and 4c show the resultant stack section and calculated Vs perturbation (dv/v) for the vertical defect synthetic model. Evident velocity perturbation artefacts appear on both sides of the perturbation peak according to the direction of the moving-source observation. In fact, when the source location is centred on the position of the defect, the waveform is perturbed for all the shot gathers even when some traces lie outside of the anomaly. To remedy this phenomenon, only the maxima of both calculated Vs perturbations (*dv/v*) of the two moving-source datasets are retained. Fig. 4c shows that the value of dv/v around -20% obtained from CCASW of the whole seismic line is coherent with the inferred true Vs perturbation value of -17%, which provides a consistency check for the method.

To characterise the in-depth velocity perturbation, a zero-phase, sine-squared, tapered band-pass filter centred on the frequencies 10 Hz to 45 Hz, in increments of 5 Hz, was applied after the cross-correlation analysis. The variables *dt* and *t* were then obtained for different frequencies of the surface wave. A “pseudo-depth” for the calculated dv/v was retrieved considering the approximation of the half wavelength of the surface wave (Wightman *et al*. 2003):

$$d = 0.53\frac{V_{ph}}{f} \qquad (3)$$

where d is the depth, Vph is the phase velocity of the surface wave, and f is the frequency. Fig. 5 shows the 2D Vs profiles reconstructed by applying the calculated lateral velocity perturbation (*dv/v*) to the homogeneous half space. Here, we observe that the CCASW allows for the reconstruction of the synthetic velocity models used for numerical modelling, and that the buried low-velocity defect is resolved using the frequency-depth conversion approximation.

Field test: Detection of a buried pipe

Data acquisition

Rayleigh wave shot gathers were acquired along a linear profile over a known buried pipe. To increase the speed and efficiency of the data recording and thereby reduce acquisition costs, a multichannel seismic cable was designed and manufactured with 24 takeouts at fixed intervals of 2 m. Each takeout is attached to a single self-orientating, gimballed, vertical geophone with a resonance frequency of 10 Hz. To ensure proper coupling, each gimballed geophone is housed in a heavy casing (~1 kg). To damp the motion of the sensor around its rotational axis, the inside of the casing is filled with viscous oil. The seismic cable was towed behind a vehicle. A 24-channel seismograph was used to record the impacts of a weight-drop electronic seismic source. The source-to-nearest-receiver offset was 2 m, whereas the source stations were separated by 10 m along the survey line. In this way, measurements were

performed with a recovering distance, as shown in Fig. 1, between each position of the seismic antenna (meaning that consecutive shots have several common geophones) to improve the signal-to-noise ratio in the CCASW stack section.

Field test: Detection of a buried karst

Geological setting

As a feasibility test of the previously outlined method, an experiment was conducted to detect a near-surface buried karst as an anomaly. The geological information is provided by 3 the geotechnical soundings performed on the investigation site (Fig. 6a):

- The levee embankment consists of loamy materials and brown silt. This formation extends vertically from the surface to a depth around 4–5 m.
- A sedimentary formation is represented by the Loire River sandy alluviums and gravels. This formation extends vertically from depths between 4–5 m to 12–13 m.

The bedrock formation is composed of differentially weathered white limestone and marls that extend to a depth around 13 m. The presence of such easily dissolved bedrock (limestone and dolomite) near the ground surface is characteristic of karst terrain. Because carbonate rocks can be dissolved by

295 groundwater, karst areas are often characterised by sinkholes, springs, and
296 underground streams whereby some surface flows are lost to groundwater
297 (Waltham *et al*. 2005; Halbecq 1996).

298

299 *Data acquisition*

300

301 Rayleigh wave shot gathers were acquired along a linear profile at the top of a
302 flood-protection levee along the Loire River in France (Fig. 6a). The survey site
303 was located in a karst terrain near an area of surface collapses (Fig. 6b), which
304 are among the known subsidence features of karst activity (Waltham *et al*.
305 2005; Halbecq 1996). The purpose of the survey was to detect potential buried
306 karstic features at the location of the collapse. The configuration used for this
307 field test is the same as that used for the detection of the buried pipe and for the
308 karst investigation in Debeglia *et al*. (2006); Which one gave good results in
309 detecting karstic features to a depth around 15-20 m Simultaneously, 3
310 geotechnical soundings (S1, S2, and S3) were performed with the aim of
311 verifying the validity and accuracy of the CCASW method.

312

313 **Results**

314

315 *Detection of a buried pipe*

316

A prerequisite to the application of the CCASW to field data was the identification of a reference shot gather that was representative of an unperturbed area for the survey line. The first shot gather was selected for the reference as it was situated at a location where no buried pipe was indicated on the pipeline plan. A CCASW stack section was then computed and a conventional dlmo processing (Park *et al.,* 1998a,b) was also applied to the entire field surface wave dataset for comparison. Fig. 7 shows the comparison between the dlmo stack section (Fig. 7a) and the CCASW stack section (Fig. 7b). The buried pipe is revealed as a diffraction at X=70 m on both stack sections. The apex of the diffraction appears at the time 0.1 s. Here, we see that the CCASW better resolves the diffraction and allows for improved accuracy and resolution compared with conventional dlmo imagery.

Detection of a buried karst

A prerequisite to the application of the CCASW to field data was the identification of a reference shot gather that was representative of an unperturbed area for the survey line. This selection was realised using the shape of the phase-velocity-versus-frequency (c-f) dispersion images. The *c-f* images of the shot gathers located near (X=280 m) and far (X=50 m) from the collapse (X=290 m) were then compared for this purpose. The c-f image of the shot gather located near the collapse (Fig. 8b) exhibited the generation of higher propagation modes, whereas this was not the case for the shot gather

340 located far from the collapse (Fig. 8a). As noted previously, the generation of
341 higher modes is a good indicator of the presence of a complex medium lying
342 below the surface location of the seismic antenna. For this field test, and in
343 many cases, we admit that the generation of higher modes in the c-f image of a
344 shot gather is an inadequate criterion for the choice of this shot gather as a
345 reference. The shot gather at location X=50 m was thus selected as the
346 reference shot for the study. Fig. 9 shows a shot gather located at X=100 m,
347 away from the collapse, a shot gather located at 280 m, and the respective
348 results of cross-correlation with the reference shot gather. A perturbation can be
349 distinguished near the collapse on the basis of the time-shifted cross-correlation
350 (approximately 0.02 s), whereas no consequent time shift is observed far from
351 the perturbed area. CCASW processing was applied to the entire field surface
352 wave dataset after a zero-phase, sine-squared, tapered band-pass filtering
353 centred on the frequencies 8 Hz to 40 Hz every 2 Hz.

354 We note that this study was conducted in the operational context of a project
355 aimed at assessing Loire River levee integrity over a total distance of
356 approximately 70 km, and we thus did not acquire surface wave data in the two
357 directions of the moving source observation. The calculated Vs perturbations
358 (*dv/v*) are then likely to be somewhat distorted compared with their true values
359 due to the effects of moving-source artefacts, as illustrated in Fig. 4.
360 Nevertheless, based on the numerical modelling results, we suggest that the
361 general distribution of velocity perturbations constitutes a reasonable first-order
362 approximation of the actual situation in the subsurface. Fig. 10 presents the
363 resulting calculated Vs perturbation (*dv/v*) for the 16 Hz frequency. Here, a Vs

perturbation (*dv/v*) of approximately -25% appears between the locations at 250 m and 300 m and almost centred on the location of the surface collapse. The frequency-depth conversion was then applied using the half-wavelength approximation, and a 2D Vs cross-section was reconstructed by applying the lateral velocity perturbations to a 1D Vs profile obtained by a non-linear least-squares inversion (Xia *et al*. 1999) of the reference shot gather dispersion curve. To ensure the correctness of reference shot gather's inversion, the authors paid attention to the fit between the observed and computed dispersion fundamental curves as in common practice in surface wave methods. A conventional MASW processing with fundamental mode inversion was also applied to the entire field surface wave dataset for comparison. Following the convention, the inverse results for each shot gather were located at the mid-point of each position of the seismic antenna. To assess the lateral variations of elastic properties with depth, the CCASW stack section was convolved with a 32-s linear sweep with frequencies decreasing from 40 to 5 Hz. This operation has the effect of separating the different frequencies of the surface wave. The frequency depth conversion was then applied using the half-wavelength approximation.

Figs 11a, 11b and 11c show the CCASW stack section and Vs profiles obtained from the MASW and the CCASW methods. The weathering index (*A-value*) curves obtained from the geotechnical soundings are superimposed on the resulting sections. This geotechnical parameter is defined as follows (Pfister 1985):

$$A = 1 + \left[\frac{POi}{PO\max} - \frac{VAi}{VA\max} \right] \qquad (4)$$

where *Poi* is the pressure on the drilling tool for depth *i*, *POmax* is the maximum pressure on the drilling tool during the sounding, *VAi* is the velocity of the drilling tool as it progresses in the ground for depth *i*, and *VAmax* is the maximum velocity of the progress of the drilling tool during the sounding; *A-values* vary between 0 for voids and 2 for highly competent materials. A coherent, weak–amplitude, low-velocity anomaly (140–300 m/s) that trends north-west from 0 to 23 m depth is evident on the convolved CCASW stack and the CCASW Vs profile and is almost centred on the location of the surface collapse (X=300 m) (Fig. 11). The attenuation area is likely caused by destructive interference due to the generation of higher modes near the location of the collapse (Fig. 8b). The anomaly decreases in coherence and magnitude down to a depth of 30 m. It is evident that the shape of the anomaly is roughly consistent with the low to very low *A-values* (0–1) from the S2 and S3 soundings, revealing the presence of highly deconsolidated materials. The *A-values* from S1, showing no dramatic values (>1) of the weathering index, reveal the relative competency of the adjacent areas. The MASW Vs profile shows a vast zone with a lower Vs (approximately 450 m/s) between the depths of 20 and 40 m and a vertical shift related to the collapsing feature (Fig. 11b). This shift is likely due to the change in the shape of the fundamental mode in the *c-f* image, which trends towards lower velocities in the perturbed area compared with the reference *c-f* image (Fig. 8). Further the velocity depression of the fundamental mode due to the presence of weathered materials, generated higher modes reveal the

complexity of the area near the collapse. Nevertheless, the velocity distribution obtained using the MASW does not coincide very well with the *A-value* curves, especially in the 10–20 m depth interval.

Discussion

The geology of the studied area consists of a levee embankment (brown silt) above a sedimentary formation that is composed of gravels and sand based on a white limestone bedrock. The CCASW stack section and CCASW Vs profile respectively reveal a weak amplitude and low velocities (approximately 140–300 m/s) in an area between 0 and 23 m deep at the location X=300 m, likely representing the complexity of the unconsolidated near surface weathered materials. The model presents significantly higher velocities in the adjacent areas. The low field velocities in the CCASW Vs profile likely result from the presence of a karstic collapse below a northwest-trending epikarst created by the flow of sediments into the karstic cavity. The MASW Vs profile shows poor agreement with the actual situation of the subsurface given by the *A-value* curves, indicating that the CCASW method greatly improves upon the accuracy and resolution of the reconstructed subsurface Vs distribution compared with the conventional surface wave methods with fundamental mode inversion. However, we note that this study considers only the fundamental mode and that the MASW Vs profile resolution could be improved when considering the recent achievements in the accurate assessment of Vs profiles using surface wave

methods. For example, further studies should compare the results of the CCASW method with the multimode inversion results of *c-f* images or joint inversion using the effective dispersion of surface waves (Hamimu *et al*. 2010).

Conclusions

The study presents the CCASW method, a novel approach to seismic imaging based on the cross-correlation analysis of multi-channel surface wave data. This method allows for high-resolution surface wav imagery and the accurate estimation of Vs perturbations and enables the reconstruction of two-dimensional subsurface Vs distribution with high resolution without requiring the systematic processes of multichannel spectral analysis of surface waves: the computation of dispersion images and the picking and inversion of dispersion curves. The overall performance of the newly developed method in this study, demonstrates that it is a simple, reliable, and very sensitive technique for characterising lateral variations in near-surface mechanical properties. This method should be applicable to the detection of a variety of subsurface defects (e.g., voids, karsts, or structural heterogeneities). The applicability of this model extends to the characterisation of material properties, integrity assessment, and surface profiling in many types of geotechnical and environmental studies. Our analyses of waveform data derived from numerical modelling and field observations indicate that the CCASW method is valid as an operational sounding method and provides strong inputs for characterisation studies of

near-surface features that allow for improved accuracy and resolution compared with conventional surface wave methods.

Acknowledgements

The study was financed by the French Research and Environment ministry. The authors thank the technicians of the BRGM for acquiring the seismic data. Finally, the authors thank the *Near Surface Geophysics* Editors, Barbara Luke and an anonymous reviewer for their comments and suggestions that led to a much-improved manuscript.

References

Bath, M. 1973*. Introduction to seismology*. John Wiley and Sons, New York.

Debeglia N., Bitri A. and Thierry P. 2006. Karst investigations using microgravity and MASW; Application to Orléans, France. Near Surface Geophysics 4, 215-225.

Foti, S., Lancellotta, R., Socco, L. V. and Sambuelli, L. 2001. Application of FK analysis of surface waves for geotechnical characterization. Fourth International Conference on Recent Advances is Geotechnical Earthquake Engineering and Soil Dynamics and Symposium in Honor of Professor W. D. Liam Finn, San Diego, California, March 26-31, 2001.

Grandjean, G. and Bitri, A. 2006. 2M-SASW: inversion of local Rayleigh wave dispersion in laterally heterogeneous subsurfaces: application to Super-Sauze landslide (France*).* Near Surface Geophysics,4, *215*-225.

Gucunski, N. and Woods, R. D. 1991. Instrumentation for SASW testing In: *Geotechnical Special Publication No. 29, Recent Advances in Instrumentation, Data Acquisition and Testing in Soil Dynamics* (eds. S. K. Bhatia and G. W. Blaney), pp. 1-16. American Society of Civil Engineers.

Halbecq, W. 1996. *Approche géomorphologique des brèches dans les levées de la Loire (Geomorphologic approach of breaches in Loire levees).* Phd thesis. Orléans, Université d'Orléans.(in French).

Hamimu, L., Safani, J. and Nawawi, M. 2010. Improving the accurate assessment of a shear-wave velocity reversal profile using joint inversion of the

effective Rayleigh wave and multimode Love wave dispersion curves. Near Surface Geophysics 9, 1-14.

Hayashi, K. and Suzuki, H. 2004. CMP cross correlation analysis of multi-channel surface wave data. Exploration Geophysics 2004 35, 7-13.

Juhlin, C. 1995. Finite-difference elastic wave propagation in 2D heterogeneous transversely isotropic media. Geophysical Prospecting 43(6), 843-858.

Levander, A.R. 1988. Fourth-order finite-difference P-SV seismograms: Geophysics 53, 1425–1436.

Miller, R.D., Xia, J., Park, C.B. and Ivanov, J.M. 1999. Multichannel analysis of surface waves to map bedrock: The Leading Edge 18, 1392–1396.

Nazarian, S., Stokoe, K.H. and Hudson, W.R., 1983. Use of spectral analysis of surface waves method for determination of moduli and thickness of pavement system. Transportation Research Record 930, 38–45.

Neducza, B. 2007. Stacking of surface waves, Geophysics 72, V51.

Park, C. B., Miller, R. D., and Xia, J., 1998a, Ground roll as a tool to image near-surface anomaly:, Society Of Exploration Geophysicists, Annual Meeting Abstracts, 874-877.

Park, C.B., Miller, R.D. and Xia, J. 1998b, Imaging dispersion curves of surface waves on multi-channel record:, Society Of Exploration Geophysicists, Annual Meeting Abstracts, 1377-1380.

509 Park, C.B., Miller, R.D. and Xia, J., 1999a, Multimodal analysis of high
510 frequency surface waves. In: *Proceedings of the Symposium on the Application*
511 *of Geophysics to Engineering and Environmental Problems* '99, pp. 115–121.

512 Park, C.B., Miller, R.D. and Xia, J. 1999b, Multichannel analysis of surface
513 waves. Geophysics 64, 800–808.

514 Pfister, P. 1985. Recording drilling parameters in ground engineering. Ground
515 Engineering 18(3), 16–21.

516 Sheu, J.C., Stokoe II, K.H. and Roesset, J.M. 1988. Effect of reflected waves in
517 SASW testing of pavements. Transportation Research Record No. 1196, 51-61.

518 Snieder. R., Grêt, A., Douma, H. and Scales, J. 2002. Coda wave
519 interferometry for estimating nonlinear behavior in seismic velocity, Science
520 295, 2253–2255.

521 Song, Y.Y., Castagna, J.P., Black, R.A. and Knapp, R.W. 1989. Sensitivity of
522 near-surface shear-wave velocity determination from Rayleigh and Love waves.
523 Technical program with Biographies, SEG, 59th Annual Meeting, Dallas, TX,
524 509-512.

525 Stokoe II, K.H., Wright, G.W., James, A.B. and Jose, M.R. 1994.
526 Characterization of geotechnical sites by SASW method. In: *Geophysical*
527 *characterization of sites, ISSMFE Technical Committee #10* (ed. R.D. Woods),
528 Oxford Publishers, New Delhi.

529 Stokoe II, K.H., Rix, G.J. and Nazarian, S. 1989. In situ seismic testing with
530 surface wave. In: *Proceedings of the XII International Conference on Soil*
531 *Mechanics and Foundation Engineering*, pp. 331-334.

Tokimatsu, K., Tamura, S. and Kojima, H. 1992. Effects of multiple modes on Rayleigh wave dispersion characteristics. Geotechnical Engineering 118(10), 1529-1543.

Virieux, J., 1986. P-SV wave-propagation in heterogeneous media: velocity-stress finite-difference method. Geophysics 51, 889-901.

Xia, J., Miller, R.D. and Park, C.B. 1999. Estimation of near-surface shear-wave velocity by inversion of Rayleigh waves. Geophysics 64, 691-700.

Xia, J., Chen, C., Tiang, G., Miller, R.D. and Ivanov, J. 2005. Resolution of high-frequency Rayleigh-wave data. Journal of Environmental and Engineering Geophysics 10(2), 99-110.

Waltham, T., Bell, F.G., Culshaw, M.G. 2005. *Sinkholes and Subsidence, Karst and Cavernous Rocks in Engineering and Construction Series*. Springer, UK.

Wegler, U. and Sens-Schönfelder, C. 2006. Fault zone monitoring with passive image interferometry. Geophysical Journal International 168, 1028-1033.

Wightman, W.E., Jalinoos, F., Sirles, P. and Hanna, K. 2003. Application of Geophysical Methods to Highway Related Problems. Federal Highway Administration, Central Federal Lands Highway Division, Lakewood, CO, Publication No. FHWA-IF-04-021.

Yanovskaya, T.B. 1989. Surface waves in media with weak lateral inhomogeneity. In: *Modern approaches in geophysics vol. 9, Seismic surface waves in a laterally inhomogeneous earth* (ed. V.I. Keilis-Borok), pp. 35-70.

Figure captions

Fig. 1 The source-receiver geometry used in the numerical tests. Both directions of the moving-source observation of surface waves were tested. The shot positions for the gathers shown in Fig. 3 are highlighted.

Fig. 2 The Vs models used for the numerical tests. The locations of the seismic antenna for the gathers shown in Fig. 3 are highlighted.

Fig. 3 A diagram illustrating the processing of surface wave data. a) Examples of the calculation of cross-correlations from the traces of a perturbed and an unperturbed shot gather with the same offset trace of the reference shot gather. In the unperturbed case, the cross-correlations are centred on the time 0 s. In the perturbed case, the cross-correlations show a travel-time perturbation of approximately 0.01 s. b) Illustration of the calculation of the Vs perturbation (*dv/v*) using equation (2) and the variables dt and t, which are highlighted by white dotted and solid lines, respectively. In the perturbed case, the Vs perturbation is approximately -10% between traces 30 and 48.

Fig. 4 a) A left-right moving source CCASW stack section for the vertical defect model. b) The calculated Vs perturbations (*dv/v*) for both moving-source directions. Velocity perturbation artefacts appear on the sides of the perturbation peak; c) The calculated Vs perturbation (*dv/v*) using only the

maxima of the calculated *dv/v* of the two moving-source datasets. The black solid line marks the real velocity perturbation of the model.

Fig. 5 The Vs profiles obtained by CCASW processing of the data obtained through numerical modelling of the synthetic models shown in Fig. 2. The locations of the seismic antenna for the gathers shown in Fig. 3 are highlighted.

Fig. 6 a) An aerial photograph of the survey site. The black solid line denotes the seismic survey line near the Loire River (France). The red dots mark the locations of the geotechnical soundings (S1, S2 and S3). b) A photograph of the collapse at the top of the flood-protection levee.

Fig. 7. A comparison of the a) dlmo stack section and b) CCASW stack section computed for field data recorded over the buried pipe. Here, we see that the diffraction due to the buried pipe is better resolved by the CCASW stack section.

Fig. 8 A comparison of the *c-f* images of shot gathers located a) far from (X=50 m) and b) near (X=280 m) the collapse (X=290 m). The reverse triangle marks the location of the surface collapse, and the black solid and black dotted lines respectively indicate the fundamental and higher propagation modes of the surface waves. The c-f image of the shot gather located near the collapse exhibits the generation of higher propagation modes, although this is not the

601 case for the shot gather located far from the collapse. The shot gather at X=50
602 m was selected as the reference shot for the study. The shot positions of the
603 gathers shown in Fig. 9 are highlighted.

604

605 **Fig. 9** The calculation of cross-correlations from traces of the unperturbed shot
606 gather (located at X=100 m) and the perturbed shot gather (located at X=280 m,
607 near the location of the collapse at X=290 m) with the same offset trace from
608 the reference shot gather (located at X=50 m). In the unperturbed case, the
609 cross-correlations are centred on the time 0 s. In the perturbed case, the cross-
610 correlations show a travel-time perturbation of approximately 0.02 s.

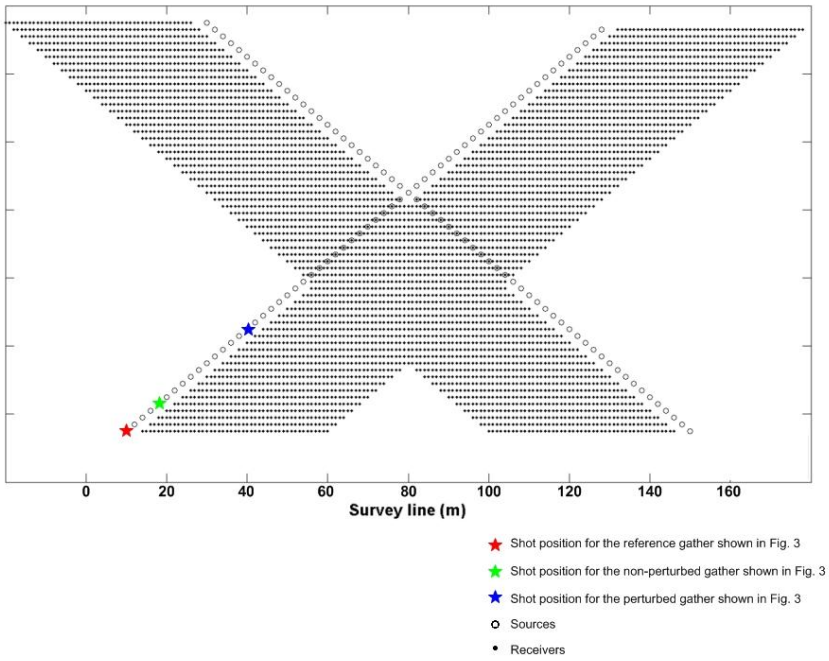
611

612 **Fig. 10** The calculation of Vs perturbations (*dv/v*) using Equation (2) for the
613 entire field surface wave dataset and for the 16 Hz frequency. A Vs perturbation
614 of approximately -20% appears in the area surrounding the collapse.

615

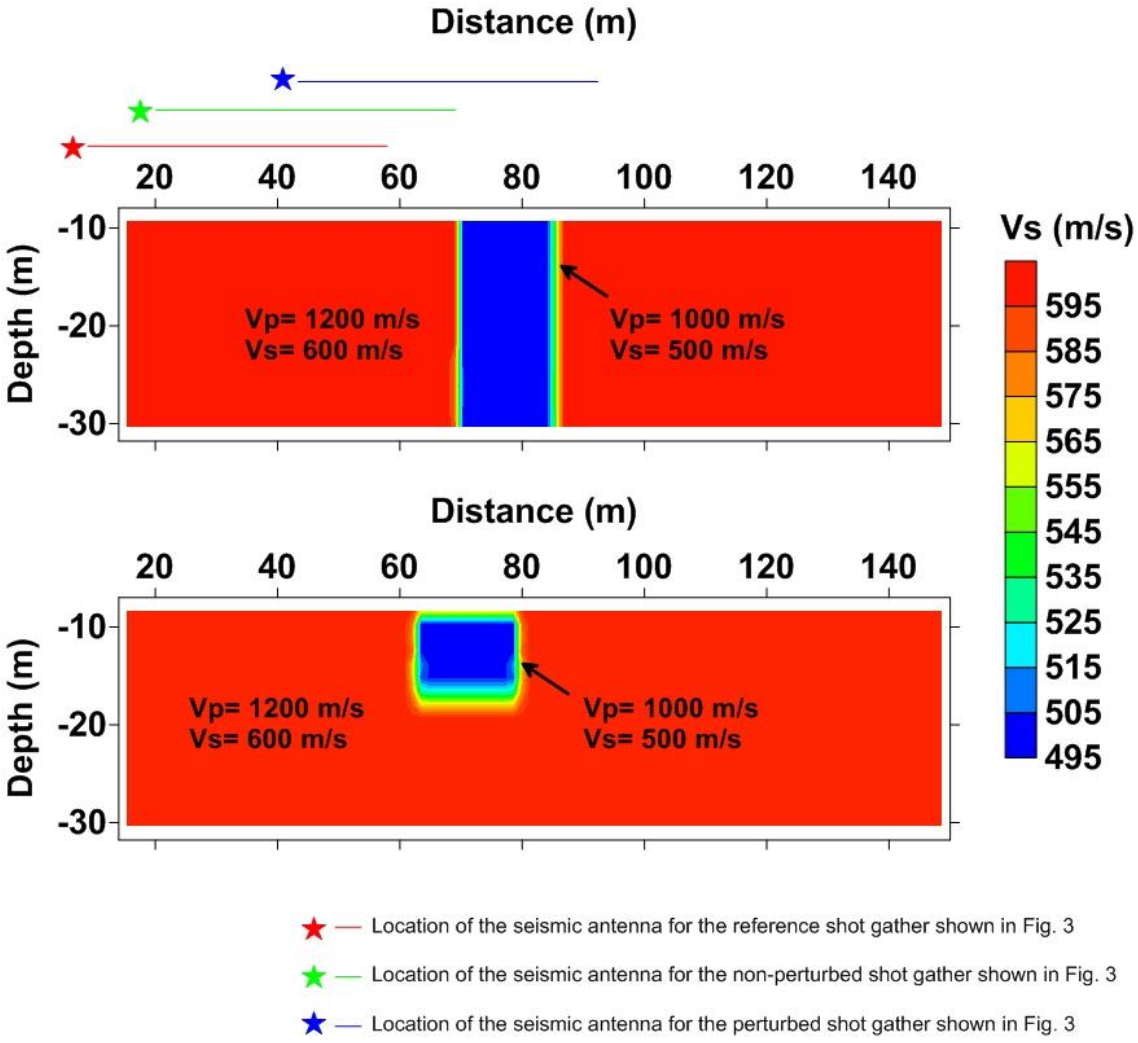
616 **Fig. 11** a) The convolved CCASW stack section. b) Vs profile defined by the
617 MASW method. c) Vs profile defined by the CCASW method. The *A-value*
618 curves overlay the profiles as solid black lines. The triangle marks the location
619 of the surface collapse. The area of attenuated amplitudes in the convolved
620 CCASW stack section is outlined by the dotted black line overlaying the Vs
621 profiles. Here, it is evident that the shape of the weak-amplitude area on the
622 CCASW stack section matches well with the low-velocity anomaly in the
623 CCASW Vs profile.

624



625

626 Figure. 1



627

628 Figure. 2

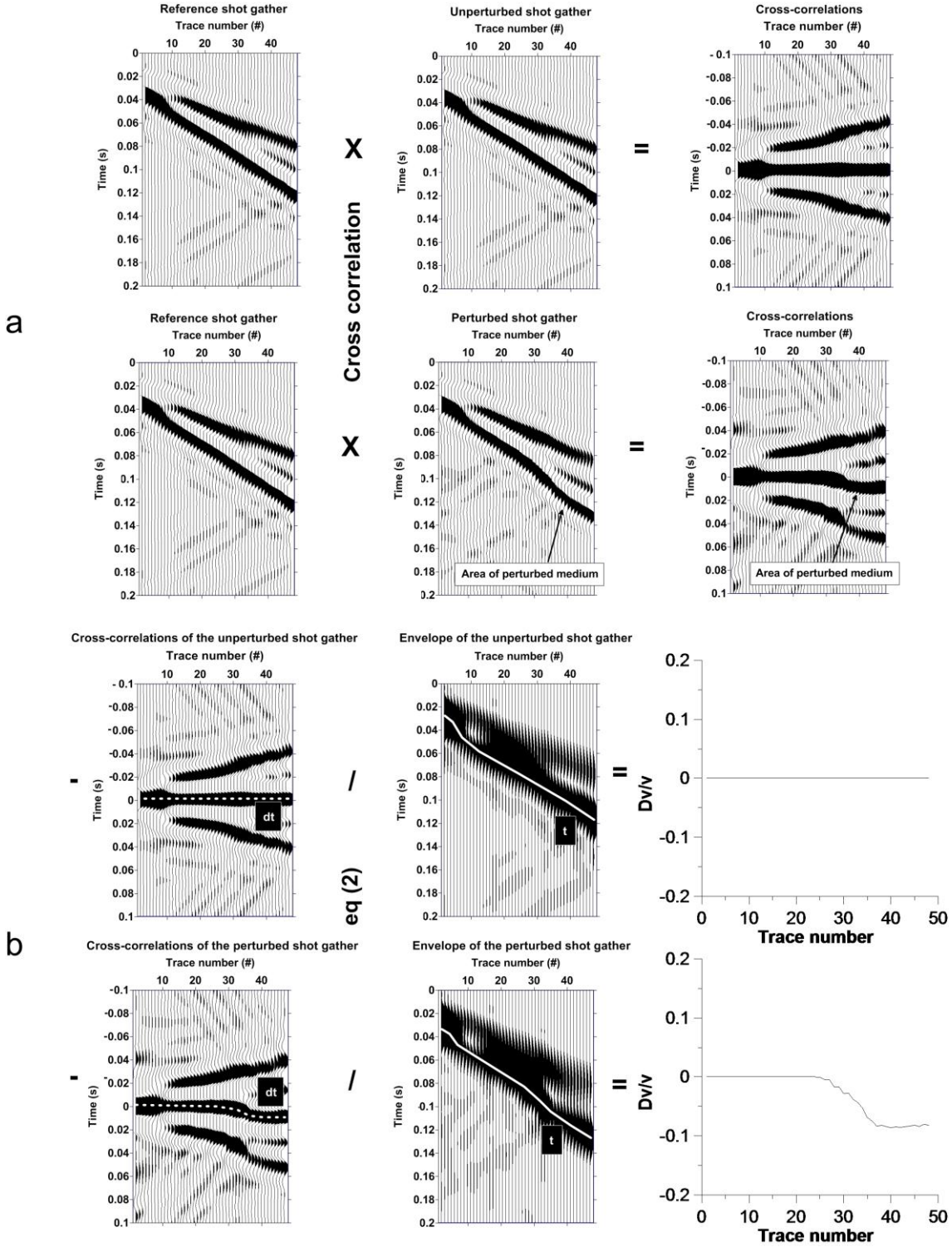
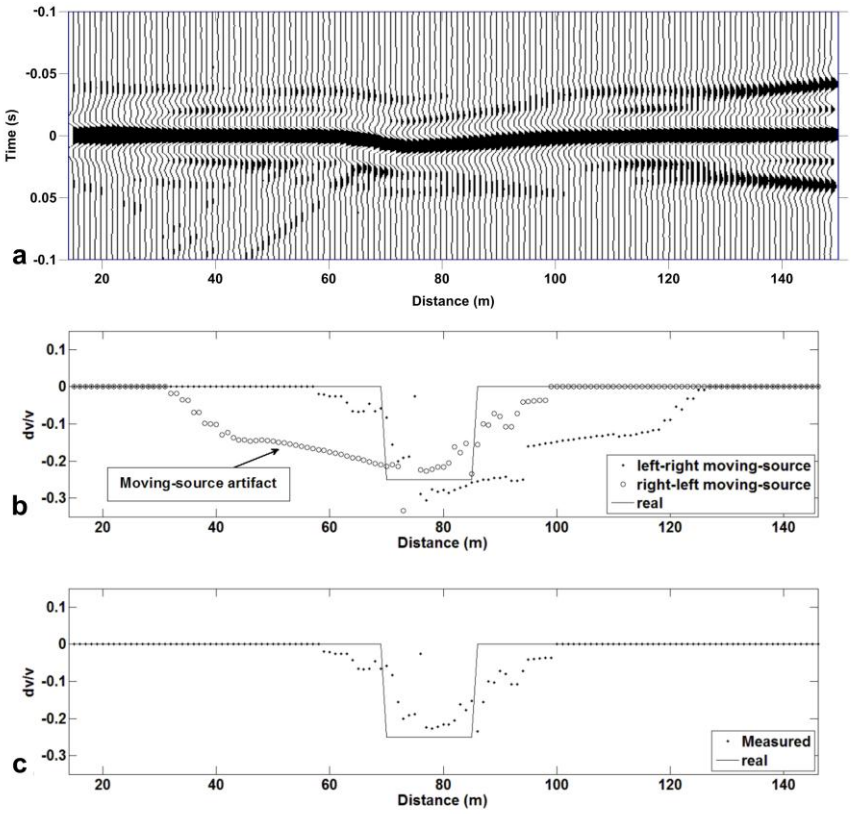
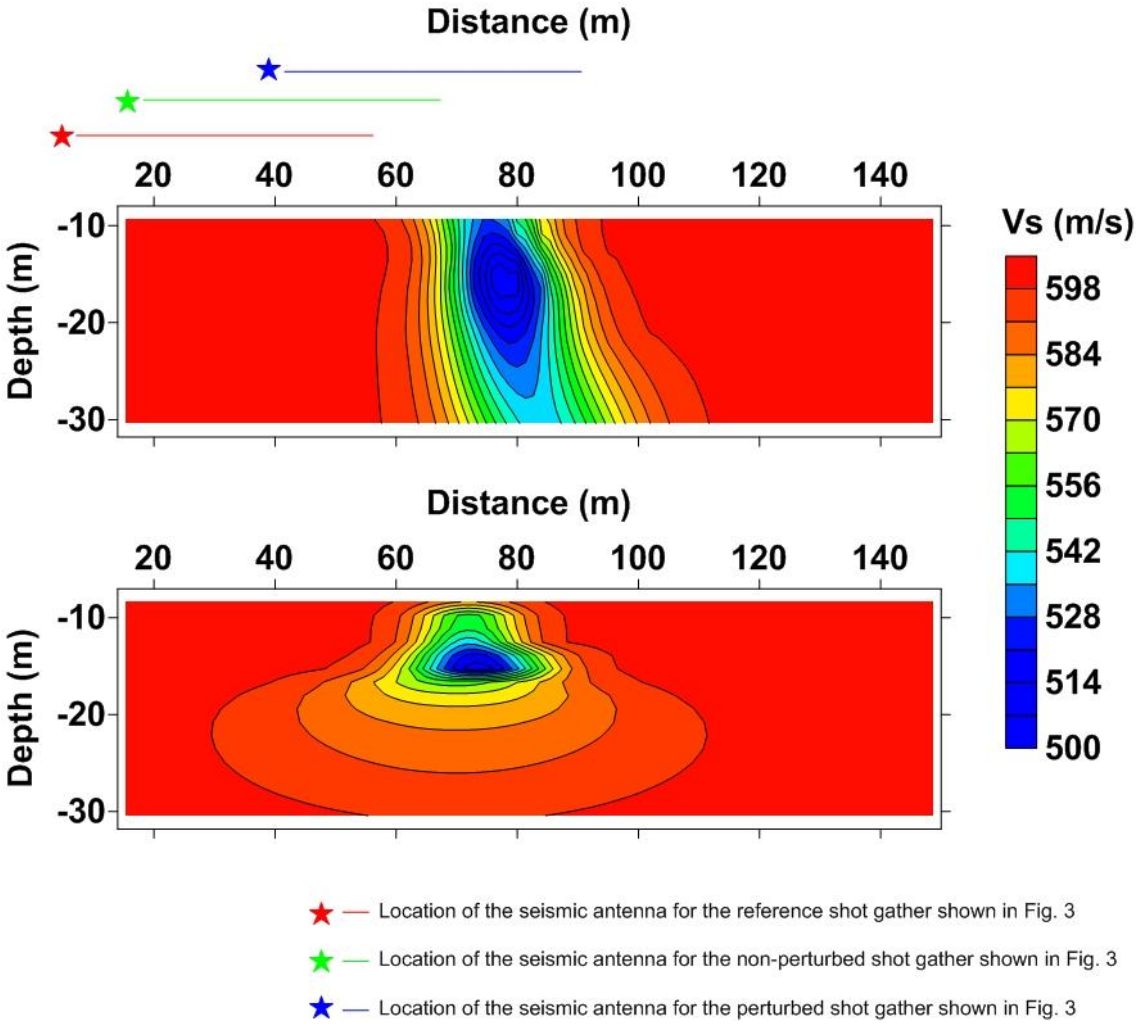

a
Reference shot gather
Trace number (#)
Time (s)
X
Cross correlation
Unperturbed shot gather
=
Cross-correlations
Reference shot gather
X
Perturbed shot gather
Area of perturbed medium
=
Cross-correlations
Area of perturbed medium
b
Cross-correlations of the unperturbed shot gather
dt
/
eq (2)
Envelope of the unperturbed shot gather
t
=
Dv/v
Trace number
Cross-correlations of the perturbed shot gather
dt
/
Envelope of the perturbed shot gather
t
=
Dv/v
Trace number

Figure. 3



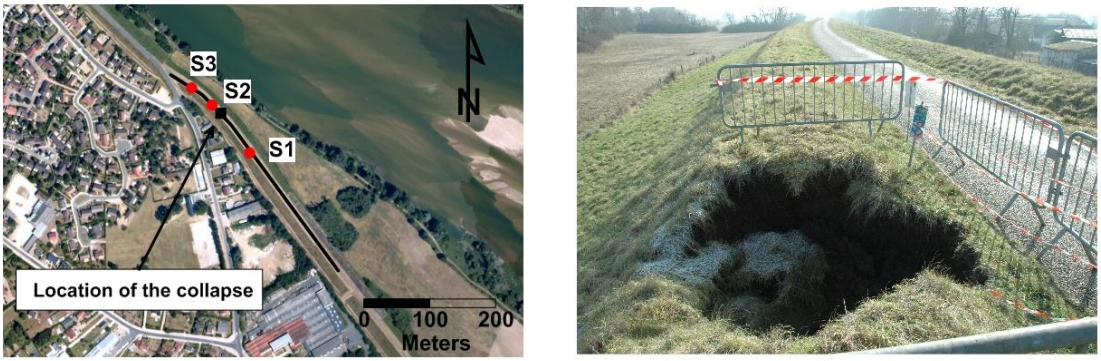
631

632 Figure. 4



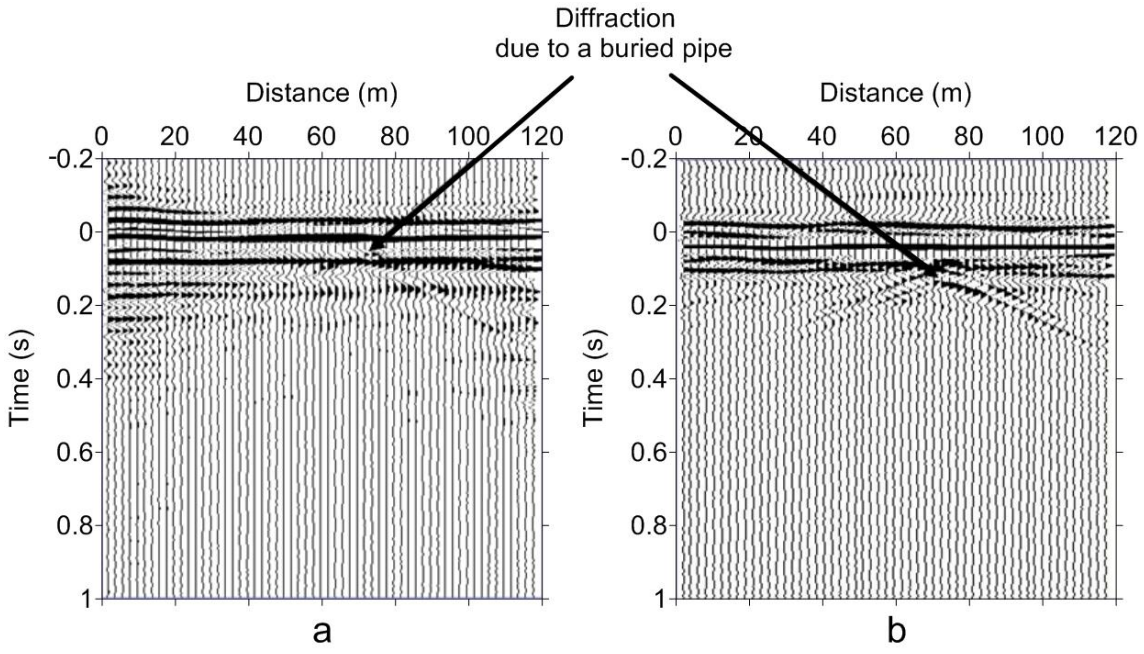
633

634 Figure. 5



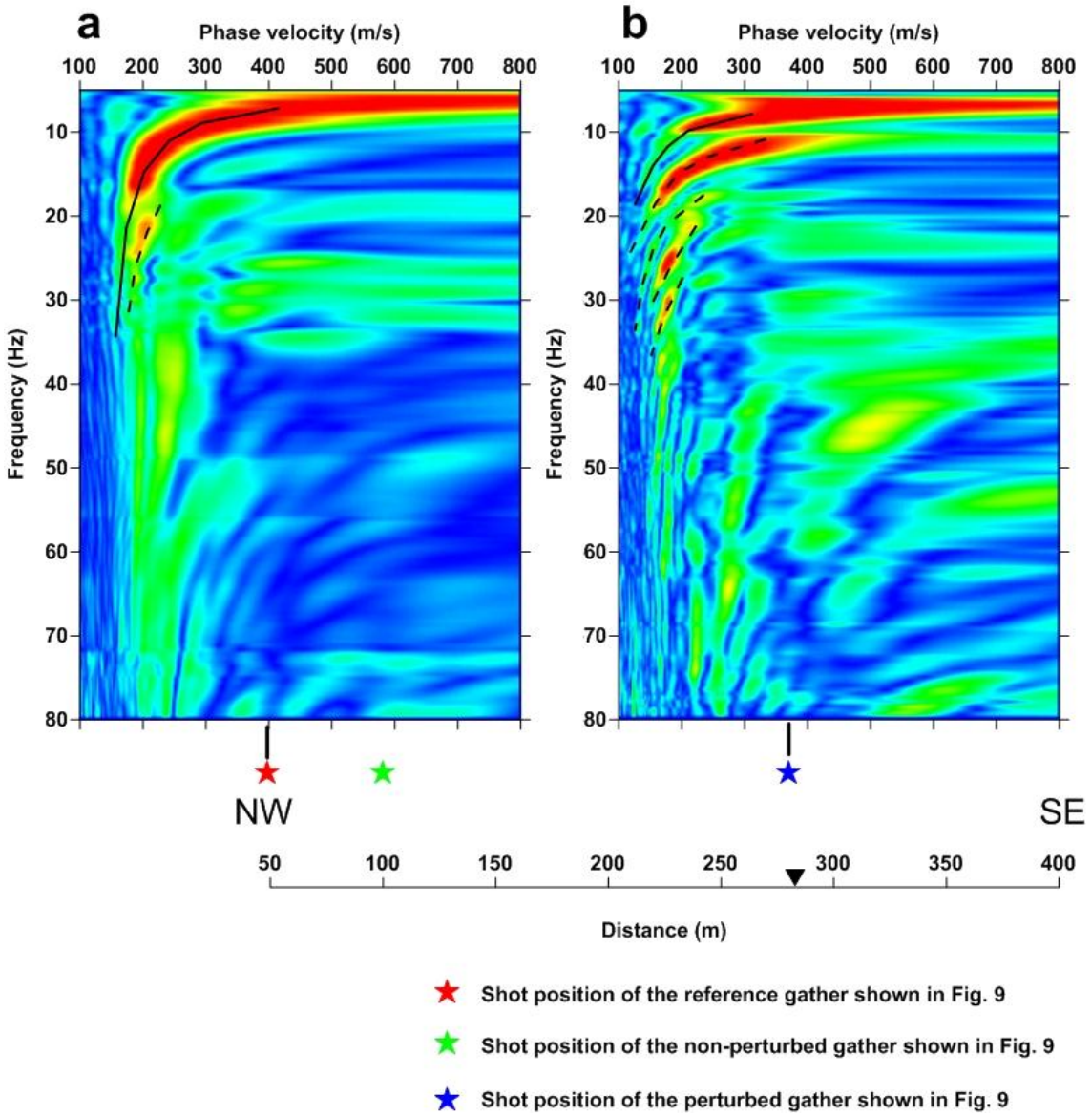
635

636 Figure. 6



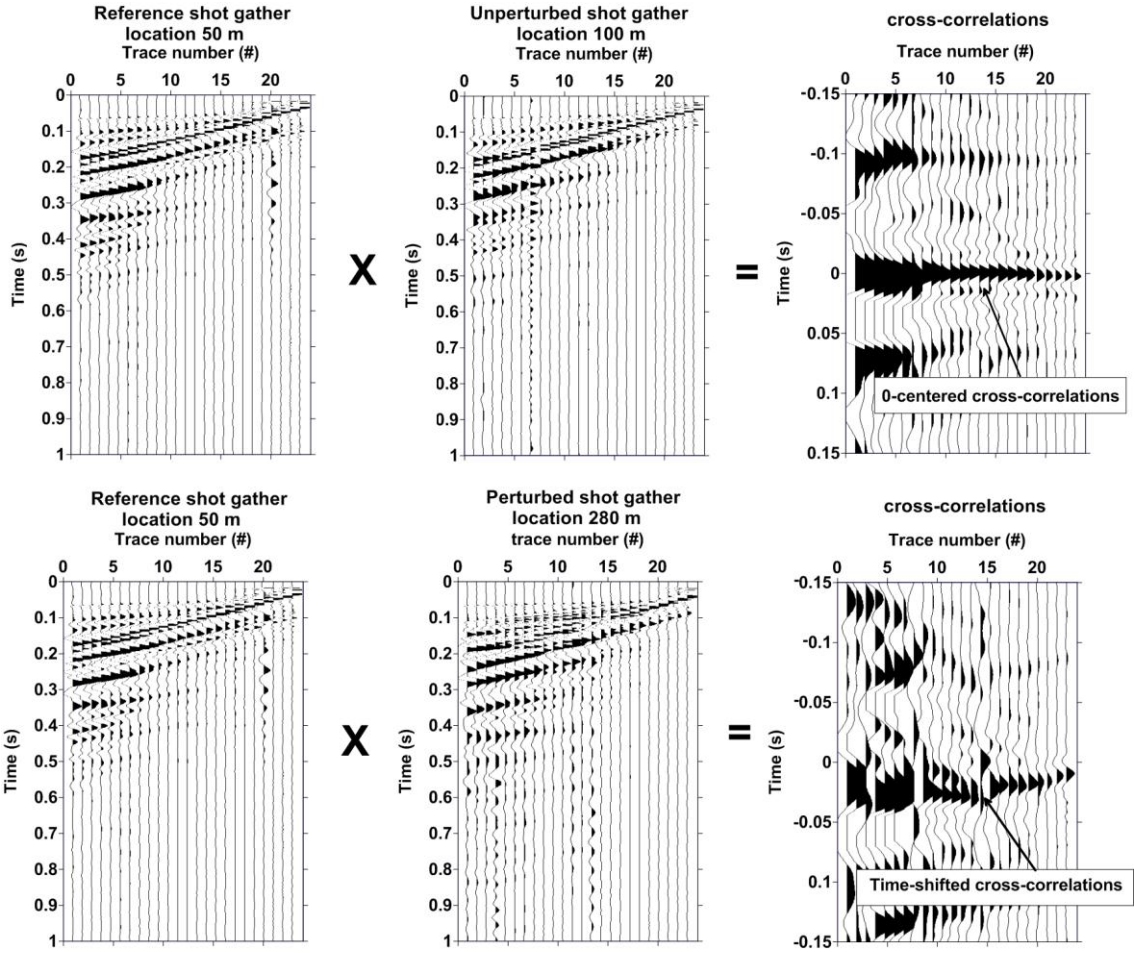
637

638 Figure. 7



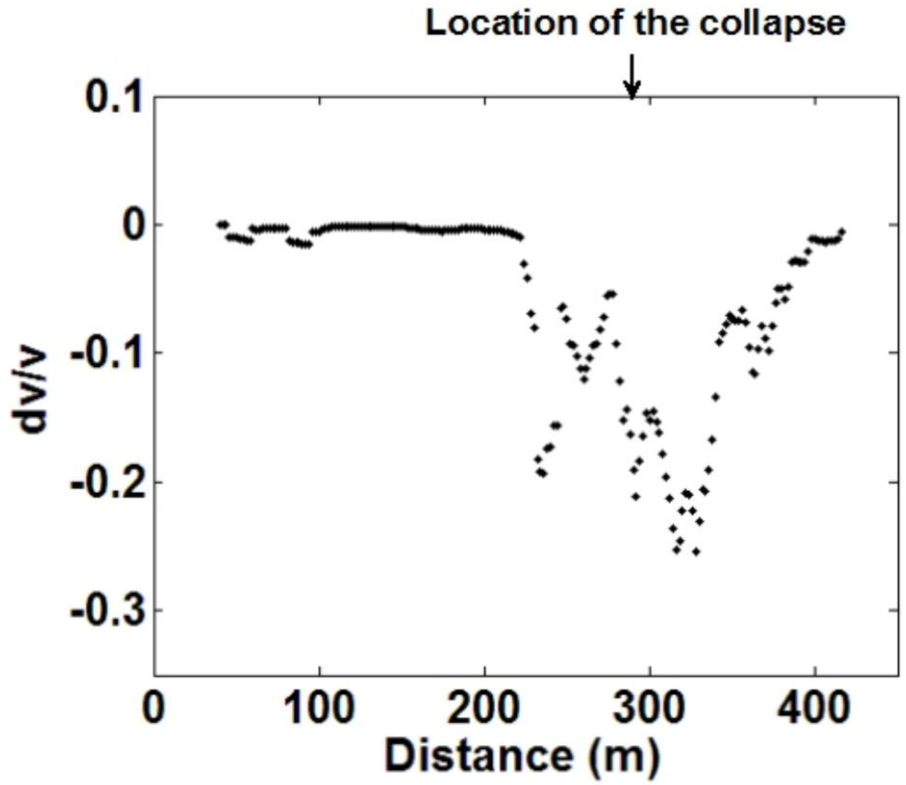
639

640 Figure. 8



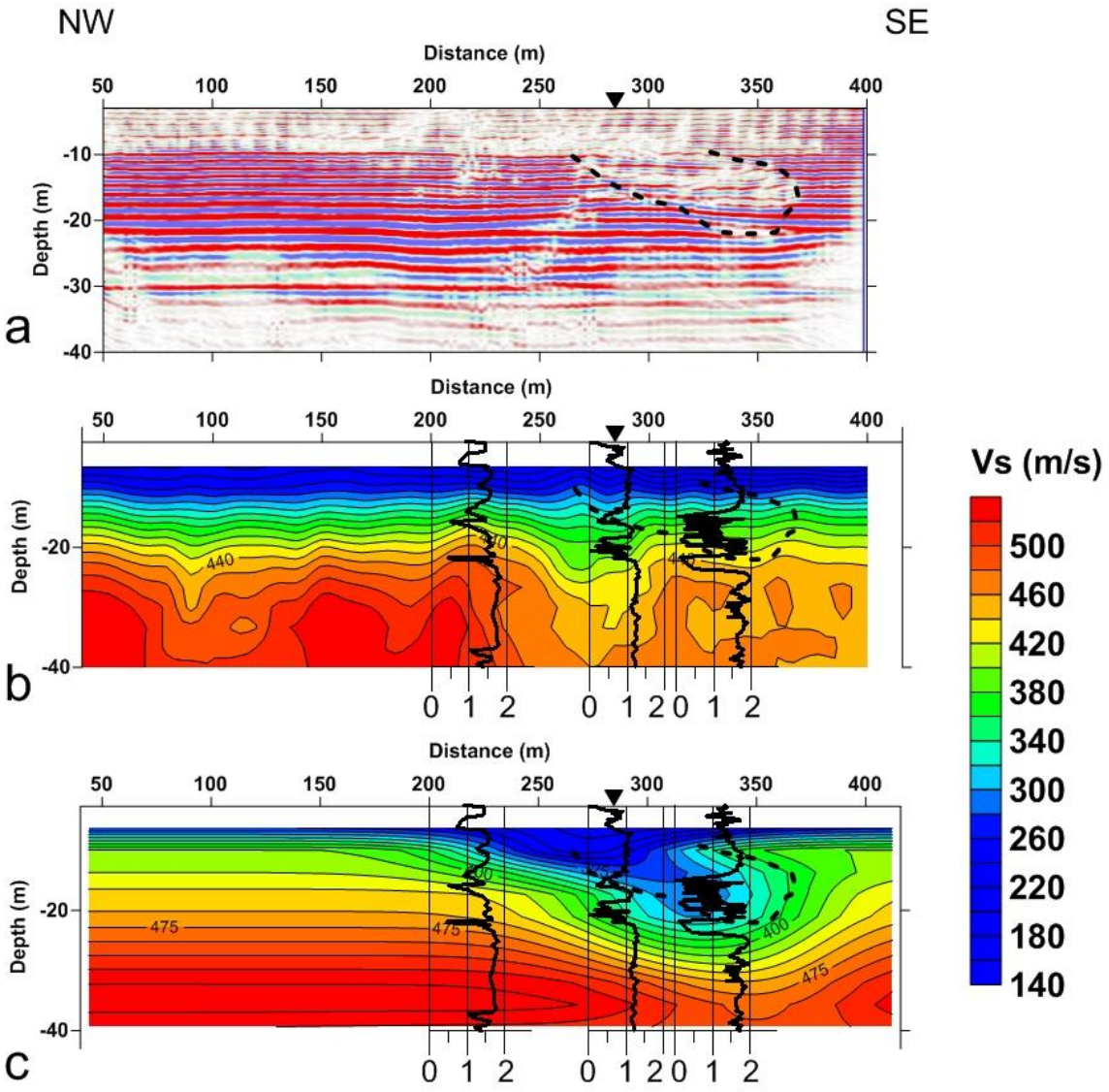
641

642 Figure. 9



643

644 Figure. 10



645

646 Figure. 11